AD-A110 903 AERONAUTICAL RESEARCH ASSOCIATES OF PRINCETON INC NJ F/G 20/4
LONG INTERNAL WAVES OF MODERATE AMPLITUDE, LAYERS OF EQUAL DEPT--ETC(U)
1982 H SEGUR, J HAMMACK

UNCLASSIFIED NL

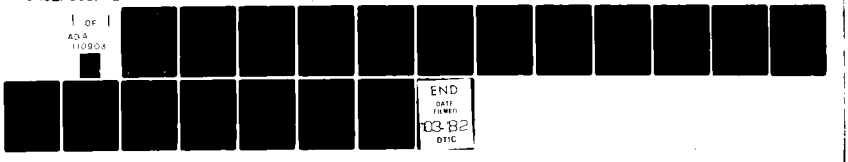

LONG INTERNAL WAVES OF MODERATE AMPLITUDE

III. LAYERS OF EQUAL DEPTH

by

Harvey Segur
Aeronautical Research Associates of Princeton, Inc.
50 Washington Road
P. O. Box 229
Princeton, New Jersey 08540

and

Joseph Hammack
Department of Civil Engineering
University of California
Berkeley, California 94720

ABSTRACT

The evolution of long, two-dimensional, internal waves of small amplitude is studied for a density stratification that excludes KdV solitary waves. Experimental data are compared with theoretical solutions of inviscid and viscous models of evolution. The inviscid model is the modified KdV equation for which dispersion and (cubic) nonlinear effects occur on a time scale even slower than that of the KdV equation. The viscous model is linear and only accounts for damping of wave amplitudes. It is demonstrated that viscosity dominates early wave evolution in the measured data. Even in these experiments, the major source of viscous effects is the interfacial shear layer; hence, the early dominance of viscosity is probable even for geophysical scale flows with one of these special stratifications. We also show that the finite thickness of the pycnocline in the experiments causes a significantly smaller phase speed than predicted by the theoretical models which utilize a two-layer approximation. A simple calculation based on a model with two homogeneous layers separated by a layer with a linear stratification accurately predicts the observed phase speeds.

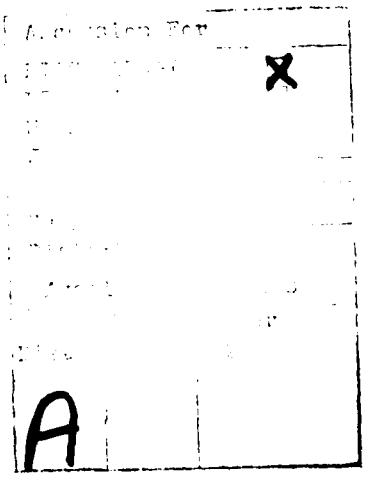

1.0 Introduction and Major Conclusions

It is well known that long internal solitary waves may occur as either waves of elevation or depression depending on the background distribution of density. (For example, see the discussion of the Korteweg-de Vries (KdV) equation in Part I of this series and references cited there.) For a density stratification separating these two wave regimes, the weak quadratic (nonlinear) interactions cancel exactly and no KdV solitary waves are possible. The purpose of this paper is to study the evolution of long, two-dimensional, internal gravity waves of small amplitude in a fluid with one of these special density distributions. Theoretical and experimental results are presented for a two-layer stratification with a small change in density across the layers. Here the quadratic interactions arising in the upper and lower layers cancel exactly when the layer depths are equal. We also note that there is a corresponding stratification for two-layers with a large change in density (Djordjevic and Redekopp, 1978) and with a continuously stratified fluid (Long, 1965 and Benjamin, 1967). To our knowledge, this is the first experimental study of wave evolution in one of these special stratifications.

Whenever quadratic interactions cancel exactly, one expects weak nonlinear effects to be dominated by cubic interactions. This is indeed the case for the two-layer system and we show that the modified Korteweg-de Vries (mKdV) equation governs inviscid evolution on a time scale that is even slower than that for the KdV equation. However, since the inviscid effects of dispersion and nonlinearity are now so weak, questions arise as to whether viscous effects still can be treated as a small perturbation on the inviscid dynamics, as they are in Parts I and II of this series. In fact,

the experimental data to be presented here indicate that the damping effect of viscosity actually dominates inviscid effects.

Motivated by experimental data, we first develop in §2 a linear model for the slow evolution of long internal waves that accounts for viscous damping but neglects both dispersion and nonlinearity. This viscous evolution model is solved for arbitrary initial data. Importantly, results here demonstrate that the unusual (dominant) role of viscosity in the experimental data is not necessarily a consequence of laboratory scale effects. The major contribution to viscous damping arises at the interfacial boundary layer rather than at the side walls of the wave tank. Hence, this effect persists even in a geophysical setting where confining side walls are absent. In §3 the mKdV equation is shown to be appropriate inviscid model for nonlinear evolution of long internal waves when layer depths are equal. Long-time solutions of the mKdV equation and its linear counterpart are presented. Finally, experimental data are presented in §4 and compared to solutions of both the viscous and inviscid models. We demonstrate that viscous effects dominate the early evolution of the measured data and that the viscous model of §2 provides a good estimate of these effects. However, both the viscous and inviscid (two-layer) models fail to predict the observed phase speed of these waves accurately. The leading order predictions of these models, which are identical, exceed measured speeds by 18%. It appears that the primary reason for the slower observed speeds is the finite thickness of the pycnocline region in the experiments. A simple calculation of phase speed based on a three-layer model with a linear stratification in the intermediate layer agrees to within 5% of the observed speed.

2.0 The Viscous Model

As already noted in Part II, the effects of viscosity on the evolution of long internal waves in a two-layer system are similar to those for long surface waves. Primary viscous effects still arise at the fluid boundaries; however, now we must include the shear layer at the fluid-fluid interface. Fortunately, the interfacial contribution is simple to include when the upper layer depth h_1 and the lower layer depth h_2 are equal, i.e. $h_1 = h_2 \equiv h$. (The notation used here conforms to that in Parts I and II.) To see this first consider a simple oscillatory wave at the interface with wave number k and frequency $\omega = ck$ where

$$c = (g\Delta h/2)^{\frac{1}{2}} \tag{1}$$

is the linear phase speed for a two-layer model, g is the gravitational force per unit mass and $\Delta=(\rho_2-\rho_1)/\rho_2$ where ρ is the mass density. (We note that the effect of any finite pycnocline thickness is to reduce the phase speed below that given by (1). The two-layer model is adopted first because of its simplicity and will be modified later to account in part for the finite pycnocline thickness in the experiments.) We assume that the wave Reynolds number satisfies $Re = \omega/\nu k^2 >> 1$ so that viscous effects are weak and boundary layers are thin. Also, we take the kinematic viscosities ν of both the upper and lower fluid to be equal which is valid for the experiments. A parameter which characterizes the magnitude of viscous effects is

$$\varepsilon_1 = \delta/h << 1 \qquad\qquad \delta = (2\nu/\omega)^{\frac{1}{2}} \tag{2a, b}$$

where δ represents the boundary layer thickness.

The leading order effect of small viscosity is an exponential damping in time (or distance) of the inviscid wave amplitude with a damping coefficient $\gamma(k)$ and e-folding time (or distance) $\gamma^{-1}(k)$. For long surface waves in a channel of breadth b, the damping coefficient, say $\tilde{\gamma}$, due to boundary

layer dissipation at the two sidewalls and bottom is (e.g., see Landau and Lifshitz, 1959, page 100)

$$\tilde{\gamma} = \left[\frac{b + 2h}{2bh}\right]\left[\frac{\nu\omega}{2}\right]^{\frac{1}{2}}. \tag{3}$$

Long internal waves experience similar viscous dissipation from the channel bottom and the portion of the sidewalls in the lower fluid layer. The added contributions due to the presence of the upper fluid layer are found by recalling from Part II that the horizontal (inviscid) fluid velocities will be equal in each layer (and oppositely directed) when the layer depths are the same. Hence, the sidewall contribution in the upper layer is identical to the sidewall effect of the lower layer. In addition, since the inviscid velocities are equal and oppositely directed above and below the interface, the actual velocity at the (quiescent) interface position is zero. The zero velocity there is equivalent to a "no slip" boundary condition, and we can imagine a (thin) solid boundary at the interface with identical boundary layers above and below. Each of these interfacial boundary layers is identical to the bottom boundary layer; hence, the total viscous effect for the internal wave is found by summing these different contributions which leads to a damping coefficient

$$\gamma(k) = \left[\frac{3b+4h}{2bh}\right]\left[\frac{\nu\omega}{2}\right]^{\frac{1}{2}} = \left[\frac{3b+4h}{2bh}\right]\left[\frac{\nu ck}{2}\right]^{\frac{1}{2}}. \tag{4}$$

(We have assumed a free surface that is fully extensible, i.e,. uncontaminated, so that no significant contribution to viscous damping arises there. This assumption appears reasonable for the experimental data presented here.) We note here that the interfacial contribution to viscous damping will generally dominate accounting for 67% of the total when $b >> h$ and exceeds 50% for $b > 4h$. In the laboratory experiments to follow the interfacial

contribution is 57% of the total based on the above analysis.

Now consider an arbitrarily-shaped one-dimensional initial wave $\eta(x,t=0)$ where x is the direction of propagation and t is time. Introducing the nondimensional variables

$$f = \sqrt{3}\ \eta/h,\ \chi = (x-ct)/h,\quad \tau = ct/6h \tag{5}$$

(for reasons that will become apparent in section 3) the initial wave becomes $f(\chi,0) \equiv f_o(\chi)$ and can be represented by its Fourier transform

$$F_o(K) = \int_{-\infty}^{\infty} f_o(\chi) e^{-iK\chi} d\chi \tag{6}$$

where $K = kh$. Assuming linear propagation of the initial wave and neglecting dispersion so that only viscous damping occurs, each Fourier component will decay with a damping coefficient (4) which can be written in nondimensional form as

$$\gamma(K) = \beta |K|^{\frac{1}{2}}, \qquad \beta = 3(3+4h/b) \left[\frac{\nu}{2hc}\right]^{\frac{1}{2}}. \tag{7a,b}$$

If $F(K,\tau)$ represents the Fourier transform of the wave system at any time τ, then the evolution equation for $F(K,\tau)$ under the above assumptions is

$$\frac{\partial F}{\partial \tau} = -\gamma F \tag{8}$$

which is easily solved.

The wave form $f(\chi,\tau)$ is recovered using the inversion integral. For initial data with $F_o(-K) = F_o(K)$, as in the experiments the final result is

$$f(\chi,\tau) = \frac{1}{\pi} \int_0^{\infty} F_o(K)\ \exp(-\beta K^{\frac{1}{2}}\tau)\ \cos K\chi\ dK\,. \tag{9}$$

We note that even though the above analysis is presented in a heuristic manner, a confirming perturbation expansion is possible following Chester (1968) and Miles (1976) who consider weak viscosity, inviscid dispersion, and nonlinearity for long surface waves.

For large times ($\tau \to \infty$), the asymptotic behavior of the solution may be found by defining

$$\xi = \chi/(\beta\tau)^{\frac{2}{3}}, \qquad \kappa = (\beta\tau)^{\frac{2}{3}}K \tag{10}$$

and expanding $F(\kappa)$ in a Taylor series about $\kappa = 0$. The dominant behavior is given by the first term in this series.

$$f(\xi,\tau) \sim \frac{F_o(0)}{\pi(\beta\tau)^{\frac{2}{3}}} \int_0^\infty \exp\left[-(\kappa\xi)^{\frac{3}{2}}\right] \cos \kappa\xi \, d\kappa \tag{11}$$

where we emphasize that $F_o(0) = \Psi$ is the nondimensional volume of the initial data taken to be finite and nonzero. If the expansion of $F_o(\kappa)$ is taken to three terms and the magnitude of the leading term is required to exceed that of the third term, a necessary condition for the validity of (11) is found:

$$\tau >> \frac{1}{\beta} \left|\frac{F_o''(0)}{2F_o(0)}\right|^{\frac{3}{2}} \tag{12}$$

where $F_o''(0) = \int_{-\infty}^{\infty} \chi^2 f_o(\chi) d\chi$ is the second moment of the initial data. (We note that the second term in the expansion always can be made zero by suitable location of the coordinate system; the criterion in (12) should be evaluated for this choice.) The viscous solution of (11) indicates that the wave form becomes self-similar for large times so that all data should collapse to a single functional form which can be represented as

$$\frac{c^2t^2}{h^3}\eta = N\left[\frac{h(x-ct)}{c^2t^2}\right] \tag{13}$$

where we have reverted to dimensional quantities.

3.0 The Inviscid Model--Modified KdV Equation

For completeness we outline here how the derivation of the KdV equation in Part I may be extended to the next slow time scale $t_2 = \varepsilon^2 t$ in order to obtain significant nonlinear effects for the case of equal-layer depths.

The necessary assumptions are:

i) $h_1 = h_2 \equiv h$

ii) $\varepsilon_2 = kh \ll 1$

iii) $\varepsilon_3 = \bar{\eta}/h \ll 1$

iv) $\varepsilon \equiv \varepsilon_3 = O(\varepsilon_2)$

v) $\varepsilon_1 \ll \varepsilon^2$

vi) the wave is strictly one-dimensional

where $\bar{\eta}$ is a characteristic wave amplitude. With these assumptions and invoking the Boussinesq approximation ($\Delta \to 0$, $g \to \infty$ so that Δg is finite) the leading order equations are the same linear hyperbolic system discussed in §2.1 of Part I. Secular terms do not occur at the next order $O(\varepsilon)$ but do arise at $O(\varepsilon^2)$, corresponding to evolution on the slow time scale $t_2 = \varepsilon^2 t$. The dimensional equation for the rightward-running wave on this time scale is

$$\frac{1}{c}\frac{\partial \eta}{\partial \tau} + \frac{\partial \eta}{\partial x} - 3\left(\frac{\eta}{h}\right)^2 \frac{\partial \eta}{\partial x} + \frac{h^2}{6}\frac{\partial^3 \eta}{\partial x^3} = 0 \tag{14}$$

To reduce (14) to standard form we introduce the nondimensional variables in (5), so that (14) becomes

$$f_\tau - 6f^2 f_\chi + f_{\chi\chi\chi} = 0 \tag{15}$$

Djordjevic and Redekopp (1978) noted that there are no soliton solutions of (15) that decay for $|\chi| \to \infty$ since the cubic nonlinear term and the dispersion term have opposite signs. The long-time solution of (15) was given by Ablowitz, Kruskal, and Segur (1979). For time τ sufficiently large the solution near the wave front is approximated by

$$f(\chi,\tau) \sim (3\tau)^{-\frac{1}{3}} W\left(\chi/(3\tau)^{\frac{1}{3}}\right) + O\left((3\tau)^{-\frac{2}{3}}\right) \tag{16}$$

where W(z) is the second Painleve function defined by ordinary differential equation

$$\frac{d^2W}{dz^2} = zW + 2W^3; \tag{17}$$

the boundary condition for (17) is

$$W(z) \sim rAi(z) \text{ as } z \to \infty$$

where

$$r = \tanh \Psi. \tag{18}$$

In dimensional terms (16) becomes

$$\eta(x,t) \sim h\left(\frac{2h}{ct}\right)^{\frac{1}{3}} W\left(\frac{x-ct}{h(ct/2h)^{\frac{1}{3}}}\right). \tag{19}$$

If the dimensionless wave volume, Ψ, is sufficiently small, then r in (18) may be expanded in terms of its argument. In addition, W(z) reduces to Ai(z) so that (19) is approximated by

$$\eta(x,t) = \frac{h\Psi}{3}\left(\frac{2h}{ct}\right)^{\frac{1}{3}} Ai\left(\frac{x-ct}{h(ct/2h)^{\frac{1}{3}}}\right). \tag{20}$$

We note that (20) is also the long-time solution of the KdV model, which reduces to a linear equation for this special stratification. Even if the wave volume is not small, both (19) and (20) predict that the wave front becomes self-similar with the same similarity variable; i.e.,

$$\left(\frac{ct}{2h}\right)^{\frac{1}{3}} \frac{\eta}{h} = N\left[\frac{x-ct}{h(ct/2h)^{\frac{1}{3}}}\right] \tag{21}$$

as $\tau \to \infty$ with only the function N differing between solutions.

4.0 Comparison with Experiments

In order to test the theoretical results of sections 2 and 3, a series of experiments was conducted following the procedures discussed Part I with h = 5 cm and $\Delta = 0.052$. The measured density stratifications at the beginning and end of the experimental series are shown in figure 1. Note

that the pycnocline thickness initially is about 1cm but increases to approximately 4 cm before the end of the experimental series. (The increase in pycnocline thickness results primarily from molecular diffusion as shown by Hammack, 1980.) The initial wave for this series of experiments is rectangular in shape with a length of 122 cm and an amplitude of 0.25 cm. Temporal records of the interface elevation were measured at five positions downstream of the generation region at 3 m intervals.

We now estimate time scales, based on a dominant length scale of $k_o^{-1} \sim 122$ cm, and an amplitude scale of $\bar{\eta}_o \sim 0.25$ cm. A characteristic (fast) time scale is $\omega_o^{-1} = (k_o c)^{-1} \sim 11$ secs. The three parameters characterizing viscous damping, inviscid dispersion, and nonlinearity, for the initial wave become, respectively,

$$\varepsilon_1 = \bar{\eta}_o/h \sim 0.094 \qquad \varepsilon_2 = k_o h \approx 0.041 \qquad \varepsilon_3 = \eta_o/h \approx 0.050. \tag{22}$$

Hence, representative measures of the slow time scale for significant viscous damping may be taken as the e-folding time $\gamma^{-1}(k_o) \approx 130$ secs (using (4) with $b = 39.4$ cm and $\nu = 0.01$ cm^2/sec) or the unit slow time scale $(\varepsilon_1\omega_o)^{-1} \approx 120$ secs. This slow time corresponds to a propagation distance of about 10 m which is within the 15 m range of experimental measurements. Alternatively, a unit of the slow time scale for nonlinearity (and dispersion) to become important is $(\varepsilon_3^2\omega_o)^{-1} \approx 1$ hour! Clearly then, viscous effects should dominate wave evolution over the range of experimental measurements. In figure 2, the waves measured at the last three downstream positions (x = 9m, 12m, and 15m) are compared with theoretical predictions based on the viscous model (9), which is evaluated numerically. The theoretical results agree fairly well with the measured data in terms of the amplitude and length scale of the dorminant portion of the evolving wave. The major discrepancy between theory and experiment occurs in the arrival times

of the wave at the downstream positions. Measured arrival times at each location correspond to an average phase speed that is 18% smaller than that of the theoretical model; we will return to this discrepancy shortly. We have also plotted the measured wave data in figure 3 in terms of the similarity variables (13) for asymptotic viscous decay. Obviously, the data have not achieved asymptotic behavior even though they do appear to be merging into a single functional form.

To reinforce our hypothesis that viscous decay dominates both nonlinearity and dispersion for this experiment, we show in figure 4 the measured data at the last three stations in terms of the inviscid similarity variables (21). The data exhibit similar trends but clearly have not collapsed into a single functional form. Figure 4 also shows the theoretical solutions (19) and (20) for the asymptotic structure of the wave front. The differences between the measured data and the (similar) theoretical solutions are striking. Predicted amplitudes exceed measurements by 500% while the predicted length scales are about 50% smaller than those measured. (As in the viscous model, the predicted phase speed is 18% greater than that measured.)

Both the viscous and inviscid models discussed above predict a leading order phase speed given by (1) which exceeds the observed speed by 18%. The disagreement between data and theory seems to be primarily a consequence the two-layer approximation, which ignores the finite thickness of the actual pycnocline region. In fact, the experimental data presented here were obtained within one and one-half hours of the final density stratification shown in figure 1, where the pycnocline thickness is approximately 4 cm or 40% of the total fluid depth. As a first approximation, the effect of the

pycnocline thickness can be estimated by using a three-layer model in which two homogeneous layers of depths $(h-\lambda)$ are separated by an intermediate layer of thickness 2λ in which the Brunt-Väisälä frequency N is constant, with

$$N^2 = \frac{g}{\rho}\frac{d\rho}{dz} = g\Delta\rho/2\lambda. \tag{23}$$

In the Boussinesq limit, N = constant corresponds to a linear change in density in the intermediate layer. The dispersion relation for this three-layer model is easily found (e.g., see Keller and Munk, 1970). For the lowest internal wave mode, the phase speed C is given by the largest root of

$$\tan(2\,N/C) = \frac{2N(\lambda-h)}{C^2-N^2(h-\lambda)^2}. \tag{24}$$

With λ = 2 cm and N = 4.8 rads/sec, which corresponds to the measured maximum N of the final stratification shown in figure 1, we find a predicted phase speed of 9.8 cm/sec compared to 11.3 cm/sec for the two-layer model and the measured speed of 9.3 cm/sec. Now the predicted and observed wave speeds differ by less than 5%. The remaining small discrepancy may be attributed to higher order effects of nonlinearity and viscosity.

The financial support for the study presented here, by the Office of Naval Research and the National Science Foundation, is gratefully acknowledged.

REFERENCES

Albowitz, M., Kruskal, M., and Segur, H. (1979). J. Math. Phys., 20, 999.

Benjamin, T. B., (1967), J. Fluid Mech., 25, p. 241.

Chester, W. (1968). Proc. Roy. Soc. London, 306, 5.

Djordjevic, V. and Redekopp, L. (1978). J. Phys, Oceanog., 8, 1016.

Hammack, J. (1980). J. Phys. Oceanog., 10, 1455.

Hammack, J. and Segur, H. (1978). J. Fluid Mech., 84(2), 359.

Keller, J. and Munk, W. (1970). Phys. Fluids, 13(6), 1425.

Landau, L. and Lifshitz, E. (1959). Fluid Mechanics, Addison-Wesley Publishing Company, Inc.

Leone, C. and Segur, H. (1981). Long internal waves of moderate amplitude, II. Viscous decay of solitons. Preprint.

Long, R. R. (1965), Tellus, 17, p. 46.

Miles, J. (1976). Phys. Fluids, 19(7), 1063.

Segur, H. and Hammack, J. (1981). Long internal waves of moderate amplitude, I. Solitons. Preprint.

LIST OF FIGURES

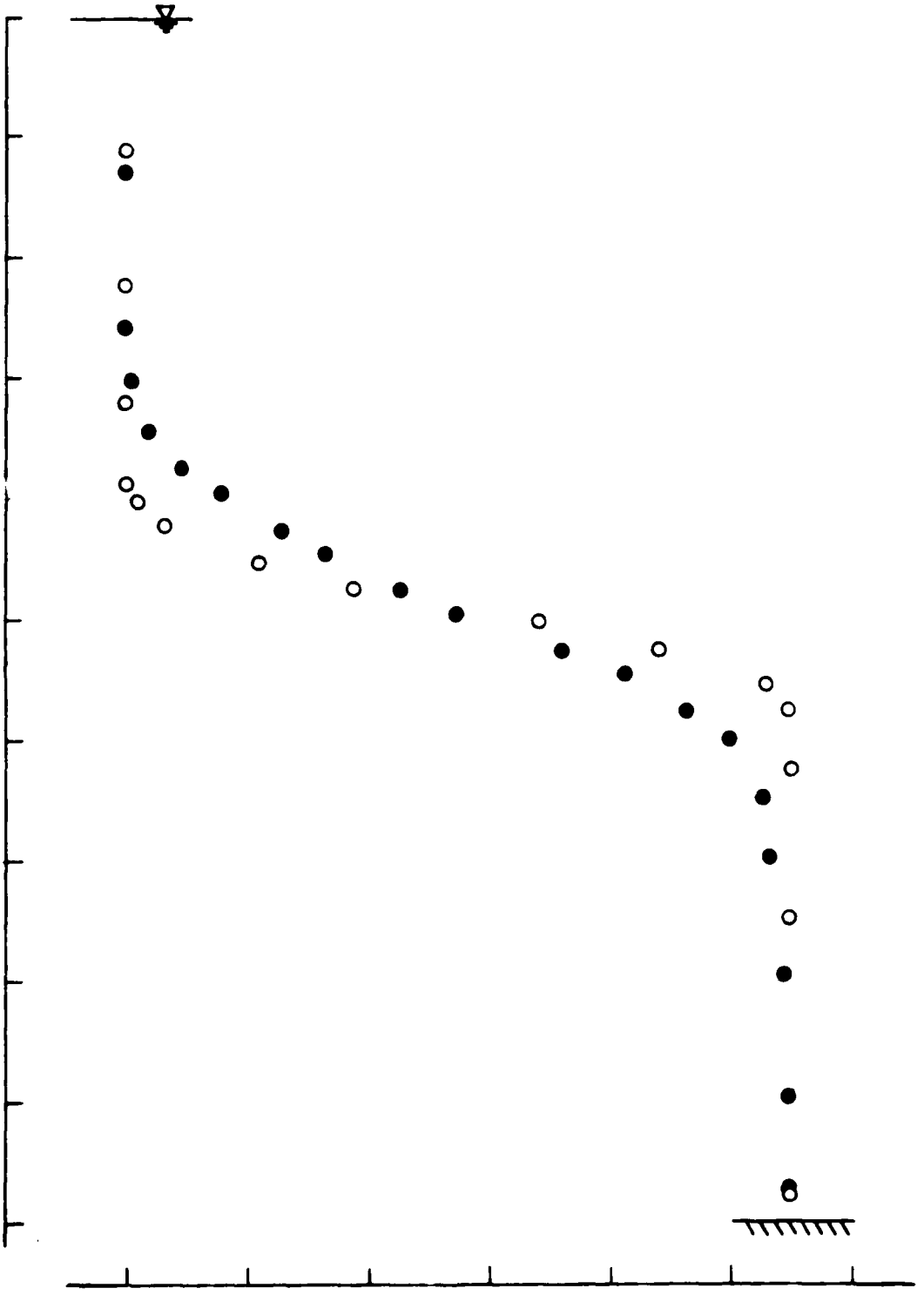

figure 1

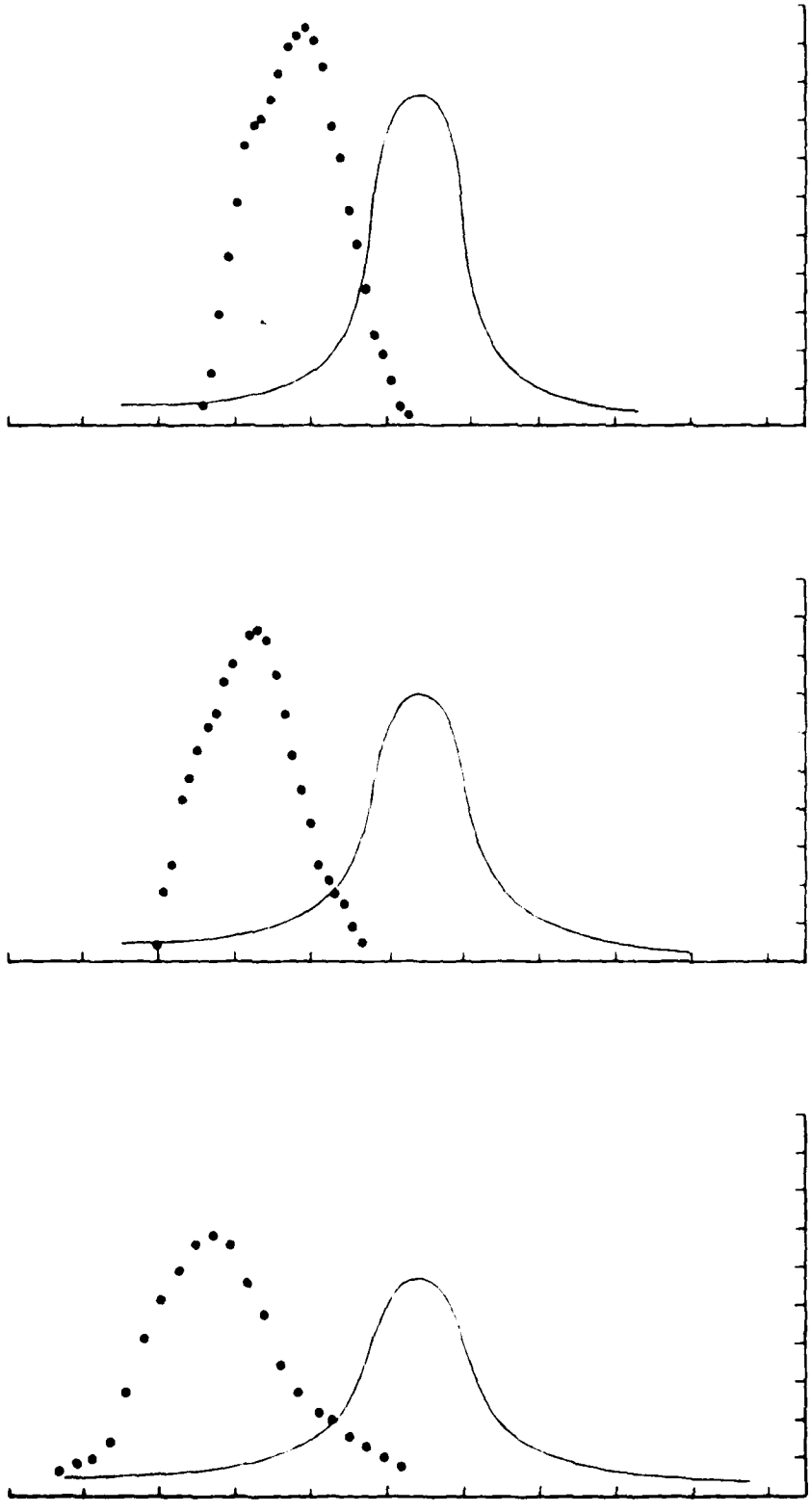

figure 2

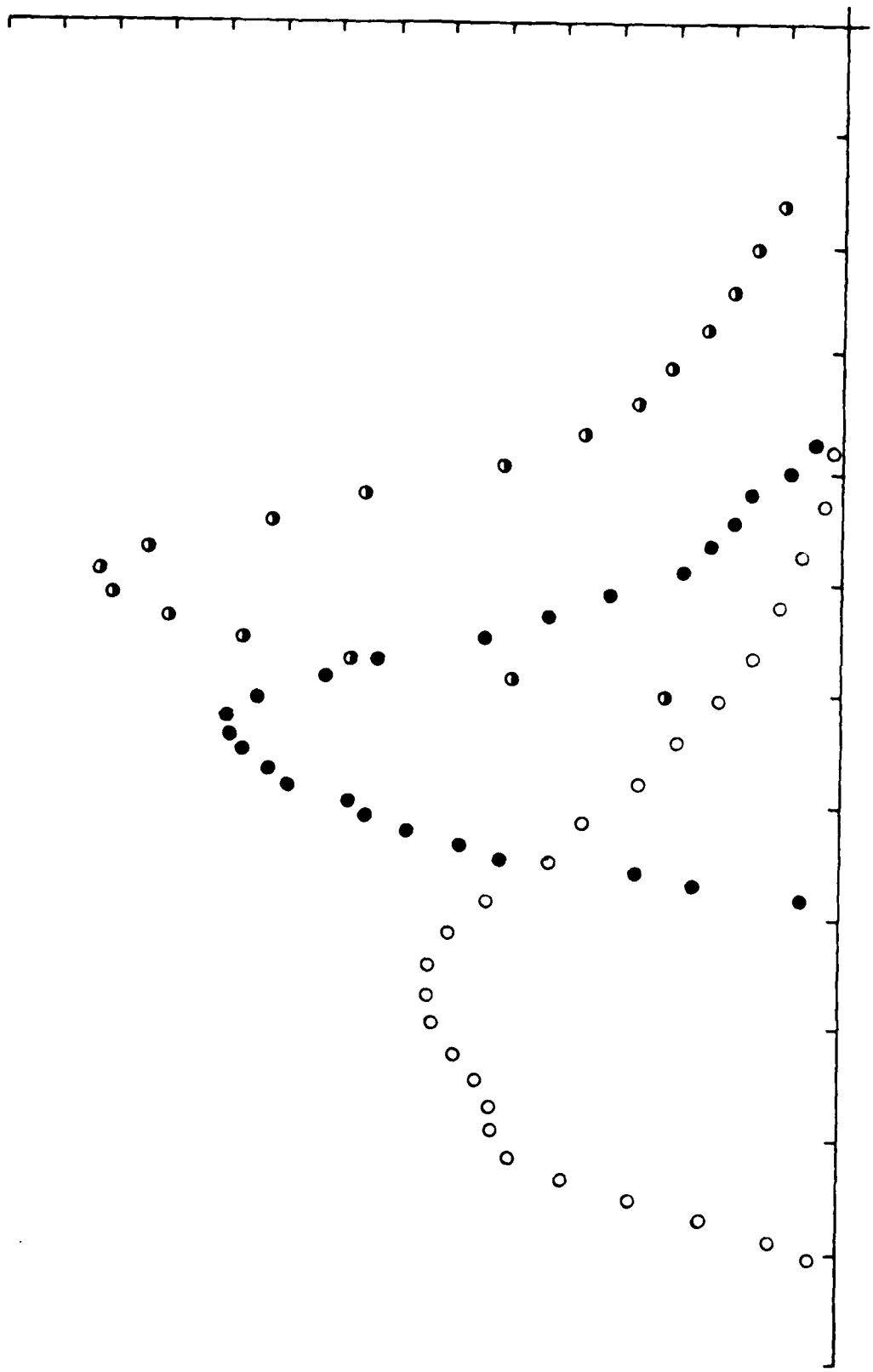

figure 3

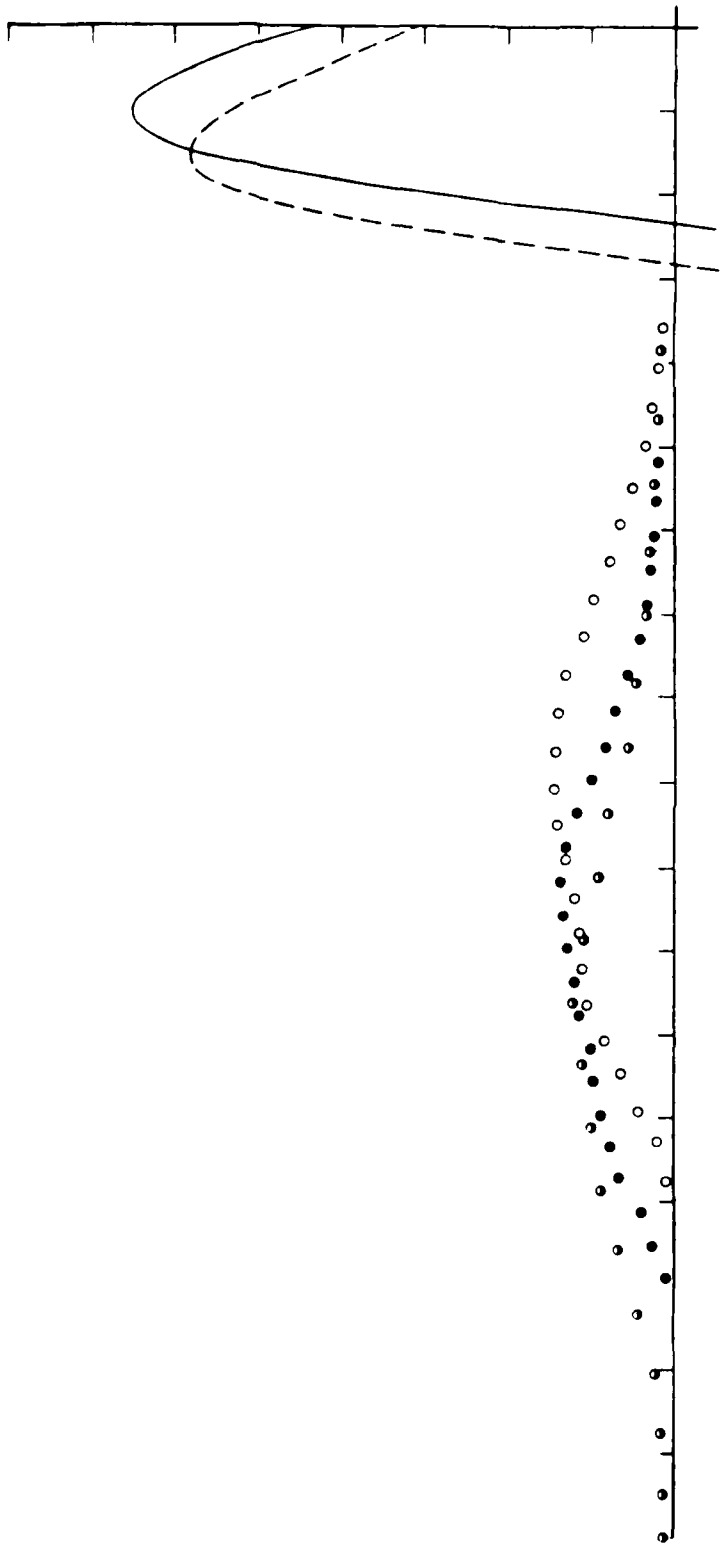

figure 4